Extended-range forecasting of stream water temperature with deep-learning models

Ryan S. Padrón[1,2], **Massimiliano Zappa**[1], **Luzi Bernhard**[1], **and Konrad Bogner**[1]

[1]Research Unit Mountain Hydrology and Mass Movements, Swiss Federal Institute for Forest,
Snow and Landscape Research WSL, Birmensdorf, Switzerland
[2]Institute for Atmospheric and Climate Science, ETH Zürich, Zurich, Switzerland

Correspondence: Ryan S. Padrón (ryan.padron@wsl.ch)

Abstract. Stream water temperatures influence water quality, with effects on aquatic biodiversity, drinking-water provision, electricity production, agriculture, and recreation. Therefore, stakeholders would benefit from an operational forecasting service that would support timely action. Deep-learning models are well-suited to providing probabilistic forecasts at individual stations of a monitoring network. Here, we train and evaluate several state-of-the-art models using 10 years of data from 54 stations across Switzerland. Static catchment features, time of the year, meteorological observations from the past 64 d, and their ensemble forecasts for the following 32 d are included as predictors in the models to estimate daily maximum water temperature over the next 32 d. Results show that the temporal fusion transformer (TFT) model performs best, with a continuous rank probability score (CRPS) of 0.70 °C averaged over all lead times, stations, and 90 forecasts distributed over 1 year. The TFT is followed by the recurrent neural network encoder–decoder, with a CRPS of 0.74 °C, and the neural hierarchical interpolation for time series, with a CRPS of 0.75 °C. These deep-learning models outperform other simpler models trained at each station: random forest (CRPS $=0.80$ °C), multi-layer perceptron neural network (CRPS $=0.81$ °C), and autoregressive linear model (CRPS $=0.96$ °C). The average CRPS of the TFT degrades from 0.38 °C at lead a time of 1 d to 0.90 °C at a lead time of 32 d, largely driven by the uncertainty of the meteorological ensemble forecasts. In addition, TFT water temperature predictions at new and ungauged stations outperform those from the other models. When analyzing the importance of model inputs, we find a dominant role of observed water temperature and future air temperature, while including precipitation and time of the year further improves predictive skill. Operational probabilistic forecasts of daily maximum water temperature are generated twice per week with our TFT model and are publicly available at https://www.drought.ch/de/impakt-vorhersagen-malefix/ wassertemperatur-prognosen/ (last access: 20 March 2025). Overall, this study provides insights into the extended-range predictability of stream water temperature and into the applicability of deep-learning models in hydrology.

1 Introduction

The services provided by streams and rivers are conditioned by water quantity and quality (van Vliet et al., 2017, 2023). For water quality, temperature is a key and highly sensitive variable, as recognized by scientists, practitioners, and regulators (Arora et al., 2016; Hannah et al., 2008; Hannah and Garner, 2015; Johnson et al., 2024; Webb, 1996). Water temperature affects the growth, reproduction, distribution, health, and survival of aquatic life (Alfonso et al., 2021; Booker et al., 2022; Elliott and Elliott, 2010; Hannah and Garner, 2015; Little et al., 2020; Singh et al., 2024), as well as dissolved oxygen (Chapra et al., 2021) and nutrient cycling (Comer-Warner et al., 2019; Johnson et al., 2024). Economic and societal aspects of electricity production, drinking-water provision, recreation, and tourism are also conditioned by water temperature (Michel et al., 2020; Ouellet et al., 2020; van Vliet et al., 2013). As we undergo the effects of the human-induced climate crisis, more frequent and new challenges related to changes in water temperature are expected

(Caretta et al., 2022; Ficklin et al., 2023; Hardenbicker et al., 2017; Michel et al., 2022; van Vliet et al., 2023).

Data-informed decisions are essential to adequately address present and future challenges associated with stream water temperature. Thus, the ongoing expansion of monitoring networks and water temperature research (Ouellet et al., 2020) provides valuable insights. While this largely applies to Europe and North America, throughout most of the world, water temperature data remain sparse, restricted, and fragmented in space and time (Ficklin et al., 2023; Hannah et al., 2011; van Vliet et al., 2023). In addition, observed and projected long-term stream water temperature regional warming trends (Arora et al., 2016; Hardenbicker et al., 2017; Kelleher et al., 2021; Michel et al., 2020, 2022) are often insufficient for stakeholders that require timely information from individual streams at a high temporal resolution. The monitoring network of the Swiss Federal Office for the Environment aims to satisfy these requirements and is used in this study to predict daily maximum water temperature across a wide range of river stations.

Stream temperatures across regions are primarily determined by climate, with air temperatures having a dominant effect. Nevertheless, the relationship between air and water temperature at individual catchments is mediated by the local meteorology, hydrology, and watershed characteristics (Hannah and Garner, 2015; Wade et al., 2023). Typically, air temperature and runoff are used to predict stream temperature (Qiu et al., 2021; Toffolon and Piccolroaz, 2015; Zhu and Piotrowski, 2020), and, less often, solar radiation, precipitation, and base flow (groundwater contribution) have also been considered (Arora et al., 2016; Feigl et al., 2021; Wade et al., 2023). The response of water temperature to changes in these environmental conditions can vary according to catchment characteristics (Wade et al., 2023). In Switzerland, the contributions of glacier or snow meltwater are relevant as they reduce the sensitivity of stream temperature to an increase in air temperature (Michel et al., 2020). Another important aspect is the shorter hydrologic residence time of small steep catchments, which hinders their ability to accumulate heat compared to larger flatter catchments that often encompass lakes. Lastly, direct human impacts from reservoir management, water withdrawal, wastewater discharge, urbanization, and so on further increase the complexity of processes influencing stream temperatures (Ficklin et al., 2023).

Statistical data-driven models are used to predict stream water temperature in an operational setting relevant to decision-making given that it is usually not possible to meet the high data requirements of process-based models to solve the energy transfer equations to and from the river (Benyahya et al., 2007; Dugdale et al., 2017; Feigl et al., 2021; Zhu and Piotrowski, 2020). Statistical models estimate water temperature as a function of related covariates and range from simple linear (auto)regression models to novel deep-learning model architectures (Corona and Hogue, 2024; Tripathy and

Mishra, 2023). The results from Feigl et al. (2021) for 10 river stations in Austria show an average mean absolute error of 0.44 °C for the best-performing machine learning models out of a set including random forest, XGBoost, feed-forward neural networks, and long short-term memory (LSTM) recurrent neural networks. These machine learning models clearly improve the prediction of daily water temperature compared to the average mean absolute error of 1.24 °C for linear regression and 0.76 °C for the Air2stream hybrid model, which combines a physically based structure with a stochastic calibration of the parameters (Toffolon and Piccolroaz, 2015). In another study with data from eight river stations in the United States, Switzerland, and China, Qiu et al. (2021) found an average mean absolute error of 0.57 °C for a deep-learning LSTM, which outperformed Air2stream, a random forest model, and a back-propagation neural network. To date, there are novel deep-learning architectures with promising results for time series forecasting (Challu et al., 2023; Lim et al., 2021; Wen et al., 2018) which are yet to be applied to forecasting water temperatures (Tripathy and Mishra, 2023).

Here, we evaluate the skill of three of these state-of-the-art deep-learning models for predicting daily maximum water temperature in 54 river stations in Switzerland over the 32 d following the start of the forecast against three more common and simpler models. An important innovation of these models is direct multi-horizon forecasting (i.e., the simultaneous prediction of multiple future time steps) instead of iteratively forecasting one day after another, which increases efficiency and robustness (Challu et al., 2023; Fan et al., 2019; Lim et al., 2021). Furthermore, some of these models produce probabilistic forecasts that are useful for risk management under uncertainty. We also assess the uncertainty stemming from the forecasts of meteorological variables that are used as predictors of stream temperature. Counting with probabilistic stream temperature forecasts over the upcoming month allows users to optimize the timing of their actions, such as adaptation measures when facing extreme conditions (Ouellet-Proulx et al., 2017). The analysis of extended-range forecasts is a novel aspect of our study that goes beyond the traditional focus on one-step-ahead forecasts. In this study, we also analyze the extrapolation capabilities of the deep-learning models to predict stream water temperature at new and ungauged stations, as well as the predictive importance of model inputs and previous time steps. Lastly, we present an example of our operational extended-range forecasts with the best-performing model.

2   Methods

2.1   Data

We use a subset of 54 stations from the Swiss Federal Office for the Environment monitoring network (https://www.hydrodaten.admin.ch/en/, last access: 2 March 2025) (Fig. 1

and Table S1 in the Supplement). Our variable of interest is daily maximum stream water temperature (WT), and for the analysis, we use data from 12 May 2012 until 31 December 2022. In addition, we employ meteorological data and information on catchment characteristics and time of the year as relevant features for forecasting stream water temperature.

The catchment characteristics from the 54 stations include catchment area, mean elevation, glacierized fraction, station coordinates, and long-term average and standard deviation of WT (i.e., target center and scale) (Table S1). The area of the catchments ranges from $3.19\,\text{km}^2$ for station 2414 (Rietholzbach – Mosnang, Rietholz) to $34\,524\,\text{km}^2$ for station 2091 (Rhein – Rheinfelden, Messstation), and the mean elevation ranges from 503 m for station 2415 (Glatt – Rheinsfelden) to 2704 m for station 2256 (Rosegbach – Pontresina). Glacierized area fraction can reach up to 24.7 % for station 2269 (Lonza – Blatten).

To provide information about the time of the year (seasonality), we define a date index (DI) as a sine function of the week of the year (woy) (Eq. 1). We construct DI to approximate 1 at the end of July (summer peak) and symmetrically decrease towards 0 at the end of January (winter peak), such that June and August or May and September have similar values. This is achieved by shifting woy by 52/12 weeks, which corresponds to 1 month. A modified date index as a predictor has been shown to improve the skill and/or training time of models (Feigl et al., 2021; Zhu and Piotrowski, 2020).

$$\text{DI} = \left| \sin\left(\pi \times \left(\text{woy} - \frac{52}{12} \right) / 52 \right) \right| \tag{1}$$

The considered meteorological variables include daily average near-surface air temperature (AT), precipitation (P), and daily fraction of sunshine duration (SD). Gridded data of these variables are provided by the Swiss Federal Office for Meteorology and Climatology at a spatial resolution of 2 km. For simplicity, we use, for each station, the time series of these variables from the single grid cell where the station is located, assuming spatial coherence between neighboring grid cells. In addition to the past observed values of these meteorological variables, their forecasts for the next 32 d are taken into account to forecast stream water temperature up to the same lead time. The meteorological forecasts correspond to a downscaled version of the extended-range forecasts from the European Centre for Medium-Range Weather Forecasts (ECMWF) that are pre-processed by the Swiss Federal Office for Meteorology and Climatology to be consistent with the gridded observations. Further details on the meteorological forecasts are provided by Bogner et al. (2022) and Chang et al. (2023), who use them for streamflow forecasting. We use ensemble forecasts with 51 members (1 control and 50 perturbed initial conditions) to capture the increasing uncertainty with lead time.

2.2 Forecasting models

We use three deep-learning models: the recurrent neural network encoder–decoder (RNNED), the temporal fusion transformer (TFT), and the neural hierarchical interpolation for time series forecasting (NHITS). In addition, we use three more common and simpler models: an autoregressive linear model with exogenous variables (ARX), a random forest model (RF), and a multi-layer perceptron neural network (MLP) with one hidden layer to put our results into context with regard to previous studies. Data from 2012 to 2021 are used for training the models, whereas data from 90 forecasts during 2022 are used for evaluating their predictions. For all deep-learning algorithms, a single general model is trained with data from all 54 stations, and daily values for the next 32 d are predicted in a single forward pass. On the other hand, the ARX, RF, and MLP models are trained separately for each station, and forecasts are produced iteratively one day at a time up to the 32 d lead time. The TFT, NHITS, RF, and MLP generate quantile forecasts of $q2$, $q10$, $q25$, $q50$, $q75$, $q90$, and $q98$, whereas the RNNED and ARX predict a single best estimate. Source code and implementations of the deep-learning models we employ are publicly available in the PyTorch Forecasting documentation (Beitner, 2020). For RF, we use the quantile regression forest implementation (Meinshausen, 2006) within the R package "ranger" (Wright and Ziegler, 2017); for MLP, we use the R package "qrnn" (Cannon, 2024); and for ARX, we use the linear model option in the scikit-learn Python tool. An overview of the forecasting models employed in this study is shown in Fig. 2.

The RNNED is a sequence-to-sequence framework based on LSTM networks to encode the history of the input sequence into a context vector and to recursively decode it into predictions (Cho et al., 2014; Hochreiter and Schmidhuber, 1997). Direct multi-horizon forecasting is performed by the decoder, generating a sequence of future predictions at once. The encoder is an RNN whose hidden state at the time step when the forecast starts is a summary c of the whole input sequence, while the decoder is an RNN that generates predictions y_t based on its hidden state h_t, the prediction of the previous time step y_{t-1}, and c. Note also that h_t itself is a function of y_{t-1} and c, as well as of h_{t-1}.

The TFT also uses LSTMs for local temporal processing in the encoder and decoder (similarly to the RNNED), but it is characterized by an attention-based architecture that integrates information from any time step and captures long-term dependencies in the data through interpretable self-attention layers (Lim et al., 2021). The multi-head attention block adds interpretability by identifying relevant time steps within the encoder period. The TFT also includes variable selection networks that, at each step, provide information about the importance of the individual predictors and allow the model to neglect irrelevant inputs. Gated residual networks (GRNs) consisting of two dense layers and an exponential linear unit (ELU) activation function (Clevert et al.,
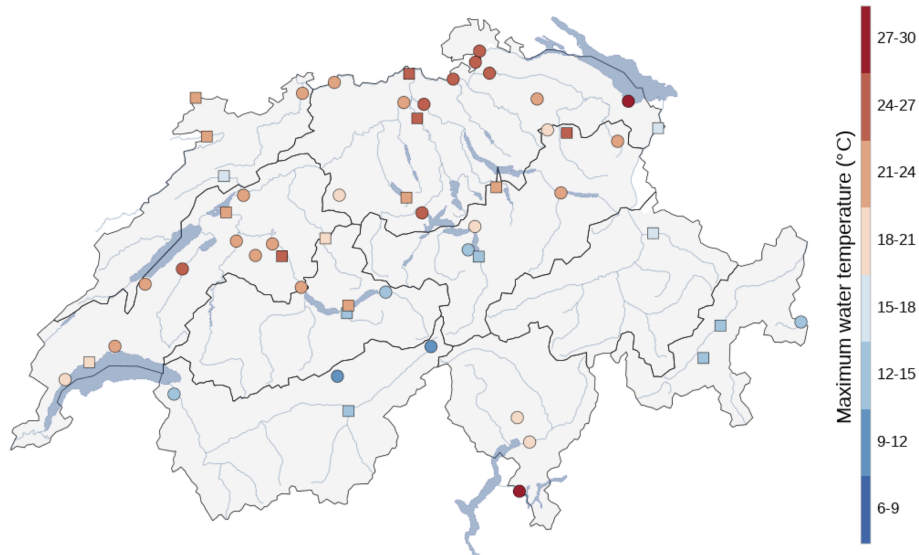
Figure 1. Map of 54 stream water temperature stations in Switzerland used for the analysis. The color bar indicates the observed mean annual maximum daily water temperature from 2012 to 2022. Squared markers indicate the subset of stations not used for training the models when evaluating the predictive skill at new and ungauged stations.
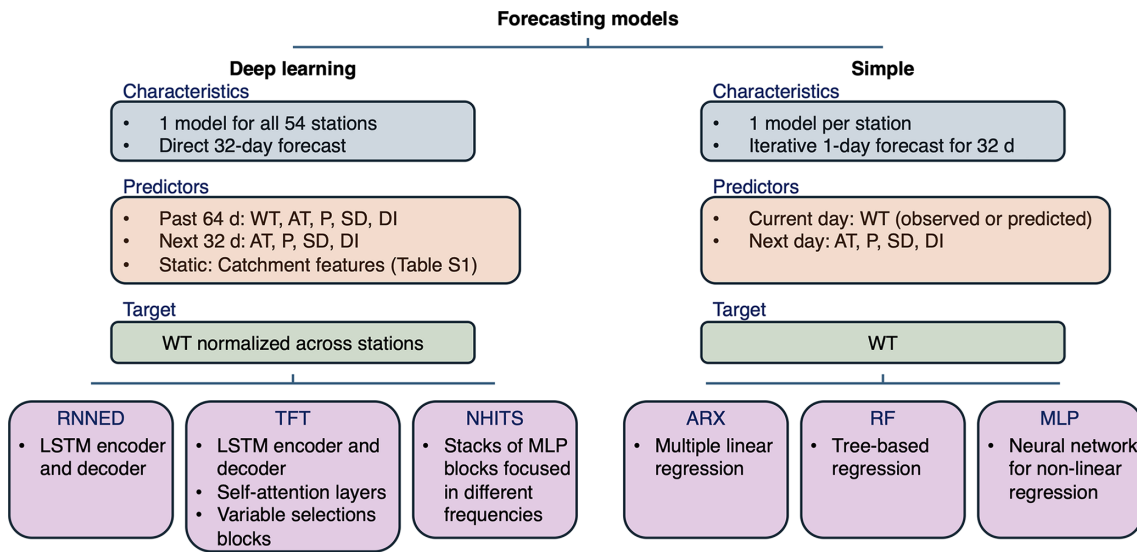
Figure 2. Overview of the deep-learning and simpler models used to forecast daily maximum stream water temperature WT. For the deep-learning algorithms, a single model is trained for the 54 stations as opposed to training one model per station. Therefore, deep-learning models include static catchment features to differentiate across stations, and WT is normalized during training.

2016) are used within the variable selection networks and elsewhere in the model architecture as gating mechanisms to adapt the model's depth and complexity according to the task at hand. Note that attention-based approaches are computationally demanding given that they can explicitly model the interaction between every pair of input–output elements (Challu et al., 2023).

Finally, the NHITS follows a different approach characterized by multi-rate sampling of the input and hierarchical interpolation of the output to increase computational efficiency,

particularly for long-horizon forecasts (Challu et al., 2023). The model is composed of stacks of MLP blocks, with each stack dealing with a different frequency (timescale) of the time series. The stacks range from those with a smooth input and low-cardinality output to those with high-frequency input and high-cardinality output. The forecast over all lead times is assembled by summing the temporally interpolated outputs of all blocks from all stacks.

For all three deep-learning models, we define the length of the encoder to be 64 d, whereas the forecasting horizon

goes up to 32 d. We use 23 different forecasts during the year 2021, with start dates that are 15 d apart from each other (i.e., 4 January, 19 January, ..., 30 November 2021), as our validation set when training the models. During each epoch of the training, 30 batches of 64 encoder–decoder chains are randomly sampled from the set of time series composed by the data of all 54 stations between 2012 and 2020. At the end of each epoch, the model parameters are updated only if they reduce the average quantile loss over all selected quantiles, lead times, and forecasts of the validation set. The quantile loss (QL) is given by Eq. (2), where q is a quantile, y is the observed value, $\hat{y}$ is the prediction, and $(.)_+ = \max(0, .)$. Note that the QL averaged over all quantile levels is an approximation of the well-known continuous ranked probability score (CRPS) (Fakoor et al., 2023; Laio and Tamea, 2007). In the case of the RNNED, we use mean absolute error (MAE) instead of QL because QL is not supported in the source code. Here, we decide to stop the training of the models if the parameters are not updated during 60 consecutive epochs, suggesting that they have converged to an optimal value. In addition, to limit computing time, we stop the training if a maximum number of 200 epochs is reached. Finally, given that the parameter optimization is not deterministic, we train each deep-learning model 10 times with a different random seed.

$$QL = q(y - \hat{y})_+ + (1 - q)(\hat{y} - y)_+ \qquad (2)$$

To train the ARX, RF, and MLP models, we use all data from 2012 to 2021 and their default settings. A least-squares fit is done for the ARX, whereas QL is used when training the RF and MLP.

2.3 Model features and hyperparameters

The deep-learning models include static catchment characteristics as predictors, given that a single model is fitted for all 54 stations. Here, we use all the static features provided in Table S1, i.e., catchment area, mean elevation, glacierized fraction, station coordinates, and long-term average and standard deviation of the target variable (target center and scale). The primary set of known time-varying model features used for the analysis includes meteorological variables and time of the year, i.e., AT, P, SD, and DI, as these are commonly available. Additional sets of model features that exclude predictors are also evaluated in Sect. 3.3. Lastly, the models also include observed WT from the encoder period.

One important aspect that influences the predictions of machine learning models is the selection of hyperparameters (Feigl et al., 2021; Kraft et al., 2025). Therefore, we conduct hyperparameter tuning for each of the deep-learning models using the Optuna framework (Akiba et al., 2019). Proposed hyperparameter values are iteratively sampled 25 times with a tree-structured Parzen estimator (Bergstra et al., 2011) that efficiently explores the hyperparameter space by focusing on the regions with the largest potential to improve the model skill, i.e., to reduce the validation loss. Additionally, hyper-band pruning is used to stop early on the iterations with hyperparameters that will not improve skill (Li et al., 2018). Details on the hyperparameters of each model, the explored hyperparameter space, and their tuned values are provided in Table S2.

The ARX, RF, and MLP models are trained per station and hence do not include static features. These models do not encode information from the recent past, and so, here, we include lagged (observed or predicted) water temperature at time $t - 1$ (lagWT) to predict water temperature at time t. The final set of features includes lagWT, AT, P, SD, and DI. The ARX has no hyperparameters. In Table S3, we explore the hyperparameter space of the RF and MLP and find that the models perform well with their default values. Therefore, we train the RF with its default values of 500 trees of unlimited depth, two out of the five features to possibly split at in each node, and a minimum node size of five data points to allow a further split. Likewise, we set the hyperparameters of the MLP to their default values of one hidden layer with two hidden nodes, a maximum of 5000 iterations of the optimization algorithm, and five trials to avoid local minima.

2.4 Forecasting at new and ungauged stations

The capability of a model to generate skillful water temperature forecasts at new locations can be of great added value for stakeholders because long-term measurements are not available everywhere (Ouarda et al., 2022). Given that deep-learning models are trained on a set of stations instead of individual time series, we expect some transferability in space to locations with similar conditions. To analyze the performance of the deep-learning models at new stations with water temperature observations and at ungauged locations, we consider models with three different setups: (A) our control model trained on all 54 stations, (B) a model trained on a subset of 34 stations with the same features as A, and (C) a model trained on a subset of 34 stations excluding past observations of water temperature from the features (i.e., ungauged). Finally, we compare the predictions of A and B, as well as of A and C, across the subset of the remaining 20 stations not used when training B and C.

We divide our data into two subsets of 34 and 20 stations with similar distributions in terms of catchment area, mean elevation, and glacierized fraction as indicated in Table S1. In addition, given that the WT long-term mean and standard deviation would not be available at new or ungauged stations, these variables can no longer be included as static features, and they cannot be used to normalize WT when training the models for setups B and C. Consequently, for setup B (new stations), we instead use the average and standard deviation of WT over the encoder period. For setup C (ungauged stations), given that we do not include past WT as a feature, we also do not include its average and standard deviation among the static features. Lastly, for each of the 20 ungauged stations in setup C, we normalize WT with data over the en-

coder period from a similar station within the subset used to train the models (Table S1).

2.5   Model performance evaluation

We use observed stream temperature from the year 2022 (excluded from model training) and 90 forecasts distributed over the year to assess the predictive skill of the models (Table S4). We do so with the continuous ranked probability score (CRPS), which is designed for ensemble forecasts (Jollife and Stephenson, 2012). The CRPS compares the cumulative distribution function (CDF) of the forecasts against the observations, and it corresponds to the mean absolute error for the case when a single value is predicted. Therefore, the units of the CRPS are those of the observed variable, with values closer to 0 corresponding to a better agreement between predictions and observations.

In our case, for each of the 51 driving meteorological forecasts, the models generate a probabilistic forecast of daily maximum water temperature given by quantiles $q2$, $q10$, $q25$, $q50$, $q75$, $q90$, and $q98$. First, for each set of quantiles, we fit a normal distribution with mean $\mu = q50$ and standard deviation $\sigma = (q90 - q10)/(\mathrm{sn}(q90) - \mathrm{sn}(q10))$, where sn(qX) corresponds to the quantile X of the standard normal distribution (i.e., with a standard deviation of 1). We then sample 100 values from each of the 51 fitted normal distributions and fit a final normal distribution to these data with parameters μ_f and σ_f. This final distribution is used when computing the CRPS according to Eq. (3), where y is the observed value (i.e., daily maximum water temperature), Φ is the CDF of the standard normal distribution, and φ is the probability density function of the standard normal distribution.

$$
\begin{aligned}
\mathrm{CRPS} = \sigma_\mathrm{f} &\left(\frac{y - \mu_\mathrm{f}}{\sigma_\mathrm{f}} \left(2\Phi \left(\frac{y - \mu_\mathrm{f}}{\sigma_\mathrm{f}} \right) - 1 \right) \right. \\
&\left. + 2\phi \left(\frac{y - \mu_\mathrm{f}}{\sigma_\mathrm{f}} \right) - \frac{1}{\sqrt{\pi}} \right)
\end{aligned} \tag{3}
$$

In addition to the CRPS, we compute the mean absolute error (MAE) and the root mean squared error (RMSE) using model estimates of $q50$ to facilitate the comparison of our results with related work according to the performance categories defined by Corona and Hogue (2024).

3   Results and discussion

3.1   Model performance comparison

We first compare the predictive skill of the models when using observed values of AT, P, and SD during the 32 d of the prediction horizon as input to generate the WT forecasts, i.e., when omitting the uncertainty of meteorological forecasts (Fig. 3). These results correspond to the best performance the models could achieve to predict water temperature by as-

suming perfect forecasts of AT, P, and SD. The TFT performs best with an average CRPS of 0.39 °C over all random seeds, lead times, stations, and forecast start dates. The other deep-learning models, namely the RNNED (0.57 °C) and the NHITS (0.60 °C), are next in line, closely followed by the RF (0.64 °C) and MLP (0.66 °C) models. For the simplest linear ARX model, the CRPS is degraded to 0.97 °C, which is 0.58 °C worse than that of the TFT. The deep-learning models show little spread in their average CRPS across the 10 random seeds: 0.014 °C for the TFT, 0.040 °C for the RNNED, and 0.022 °C for the NHITS. This suggests that the models converged to optimal parameters during training. In addition to the CRPS, we provide MAE and RMSE results in Figs. S1 and S2, respectively. Regarding the run time needed on our server to train each model for 200 epochs, the longest is 44 min for the TFT, with 286 100 parameters, followed by 21 min for the RNNED, with 60 900 parameters, and 17 min for the NHITS, with 103 800 parameters. For the simpler models, less than a minute is needed to train them at each station, and this can easily be done in parallel.

For all models, the predictive skill decreases with lead time as the influence of observed daily maximum water temperature on the predictions is also reduced (Fig. 3a). The decrease in skill is particularly fast during the first 4 d for ARX, MLP, and RF, suggesting that these models have a higher reliance on past water temperature for predicting future water temperature. Across stations, there is substantial variability in the CRPS for all models (Fig. 3b). As an example for the TFT, it ranges from 0.23 °C for station 2276 (Grosstalbach – Isenthal) to 0.74 °C for station 2068 (Ticino – Riazzino). No clear relationships emerge when evaluating predictive skill as a function of catchment characteristics such as area, elevation, and glacierized fraction (Fig. S3). Lastly, we note that the predictive skill of the models also varies seasonally (Fig. 3c). The CRPS is lower in the winter when water temperature is colder and has lower day-to-day variability, whereas it is higher in the summer when the conditions are opposite.

It is likely that stream water temperature at several of the Swiss stations analyzed in this study is influenced by reservoir and lake management (Michel et al., 2020) and potentially also by water withdrawal and discharge from industry, for example. Larger deviations between observed and forecasted values are expected when management decisions influencing water temperature take place, given that their timing can be largely arbitrary and thus not captured by our models. This seems to be the case for stations 2068 (Ticino – Riazzino), 2084 (Muota – Ingenbohl), and 2351 (Vispa – Visp), with the highest CRPS as seen in Fig. 3b. These stations are highly influenced by hydropeaking from the release of large volumes of cold water from reservoirs at high elevations (Michel et al., 2020). It is noteworthy that the high CRPS values for forecast start dates between mid-April to mid-May (Fig. 3c) are mainly driven by high CRPS values at these affected stations (Fig. S4). Furthermore, dur-

ing this time for the year 2022, the models underestimated the observed water temperatures (Fig. S5), which is a reasonable consequence if less cold water was released during the drought year 2022 compared to during past years used to train the models.

Figure 4 compares the operational predictive skill of the models when using AT, P, and SD forecasts over the 32 d of the prediction horizon as input to generate the forecasts. The TFT remains the best-performing model, with an average CRPS of 0.70 °C over all random seeds, lead times, stations, and forecast start dates, followed by the RNNED with 0.74 °C, the NHITS with 0.75 °C, RF with 0.80 °C, MLP with 0.81 °C, and ARX with 0.96 °C. When comparing these results to those from Fig. 3, we note that the uncertainty of the meteorological forecasts contributes 0.31 °C to the total disagreement between observations and TFT predictions and less for the other models. Consequently, the uncertainty of the meteorological forecasts decreases the gain in predictive skill to be achieved when using the TFT compared to the other models. This is particularly the case for lead times beyond 5 d, where there is often a strong decrease in meteorological predictability (Bauer et al., 2015).

There is an evident decrease in the predictive skill of water temperature as lead time increases (Fig. 4a), which is directly related to the ensemble meteorological forecasts being less accurate and having a larger spread for predictions further into the future. For all models, the CRPS at a lead time of 32 d is more than double its value at a lead time of 1 d. In the case of the TFT, it increases from 0.38 °C at lead time 1 to 0.90 °C at lead time 32. In addition, we find that the uncertainty of the meteorological forecasts increases the CRPS variability across stations and forecast start dates and can lead to other models outperforming the TFT in some cases (Fig. 4b and c).

High average CRPS values greater than 1 °C – even for the TFT – occur at several stations, namely 2612 (Riale di Pincascia – Lavertezzo), 2308 (Goldach – Goldach, Bleiche, nur Hauptstation), 2068 (Ticino – Riazzino), 2374 (Necker – Mogelsberg, Aachsäge), and 2112 (Sitter – Appenzell), representing a large increase compared to their values in Fig. 3 (except for station 2068, influenced by reservoir management). Therefore, these high errors in predicted water temperature arise from errors in the meteorological forecasts. It is noteworthy that the catchment area of the above-mentioned stations is less than 90 km^2 (except station 2068), and the catchment of station 2612 is particularly steep. These conditions are likely to make water temperature more sensitive to changes in AT, P, and SD – i.e., the change in water temperature per unit change in the meteorological predictors is greater (Wade et al., 2023). Indeed, Fig. S6 shows a tendency for higher CRPS at stations with smaller catchment area. Meanwhile, the high CRPS values during April and September in Fig. 4c result from the contribution of most stations (with a strong influence from station 2612) (Fig. S7). This decrease in predictive skill was caused by specific weather events that deviated strongly from the meteorological fore-

casts, particularly for lead times beyond 2 weeks (Fig. S8). Finally, in Fig. S9, we show that a similar average CRPS is obtained for the TFT if we use catchment average AT, P, and SD as predictors instead of their values in the single grid cell where the station is located, as in Fig. 4. Using catchment averages improves the predictive skill for relatively small and steep catchments with high spatial variability in terms of the meteorological conditions, such as 2612 and 2068, but it is counterproductive for large catchments such as 2392 (Rhein (Oberwasser) – Rheinau) and 2288 (Rhein – Neuhausen, Flurlingerbrücke), where the meteorological conditions tens of kilometers upstream of the station are less relevant than the conditions near the station.

Supplementarily to the CRPS information of Fig. 4, we provide the corresponding MAE and RMSE of the models in Figs. S10 and S11 to facilitate the comparison of our results with previous work. For a lead time of 1 d, all six models tested here achieve a very good performance according to the ratings suggested by Corona and Hogue (2024), while their MAE values of 0.53 °C for the TFT, 0.45 °C for the RNNED, 0.61 °C for the NHITS, 0.55 °C for RF, 0.52 °C for MLP, and 0.56 °C for ARX are similar to the 0.44 °C reported by Feigl et al. (2021) for 10 stations in Austria and the 0.57 °C reported by Qiu et al. (2021) for 8 stations in the United States, Switzerland, and China. The predictive skill for lead times beyond 1 d is a novel aspect of our study, with no previously reported values available for comparison. We note that, in terms of MAE and RMSE, the RNNED performs better than the TFT for lead times up to 7 d. This is not the case in terms of the CRPS because, for the TFT, we use the seven quantiles of the probabilistic forecast (instead of only $q50$, as for computing MAE and RMSE), whereas, for the RNNED, we only count with one best estimate available for each ensemble member of the meteorological forecasts.

3.2 Predictive skill at new and ungauged stations

Figure 5 compares the CRPS across 20 stations from predictions of deep-learning models trained either including (setup A) or excluding (setup B) data from this subset of stations. When forecasting water temperature at new stations on which the models are not trained, results show that the TFT performs best, with an average CRPS of 0.83 °C, across all 32 lead times, 20 stations, and 90 forecasts distributed over a year, followed by the NHITS, with 0.92 °C, and the RNNED, with 1.11 °C. The reduction in prediction skill when extrapolating the models to new stations is 0.11 °C for the TFT, 0.12 °C for the NHITS, and 0.34 °C for the RNNED. The larger drop in skill of the RNNED occurs at more than half of the 20 stations and throughout most forecast dates, with particularly large values at the highest-elevation stations: 2256 (Rosegbach – Pontresina) and 2462 (Inn – S-chanf). On the other hand, we note the good extrapolation capability of the TFT to new stations during the summer, with its CRPS following closely that of the TFT trained on all 54 stations.
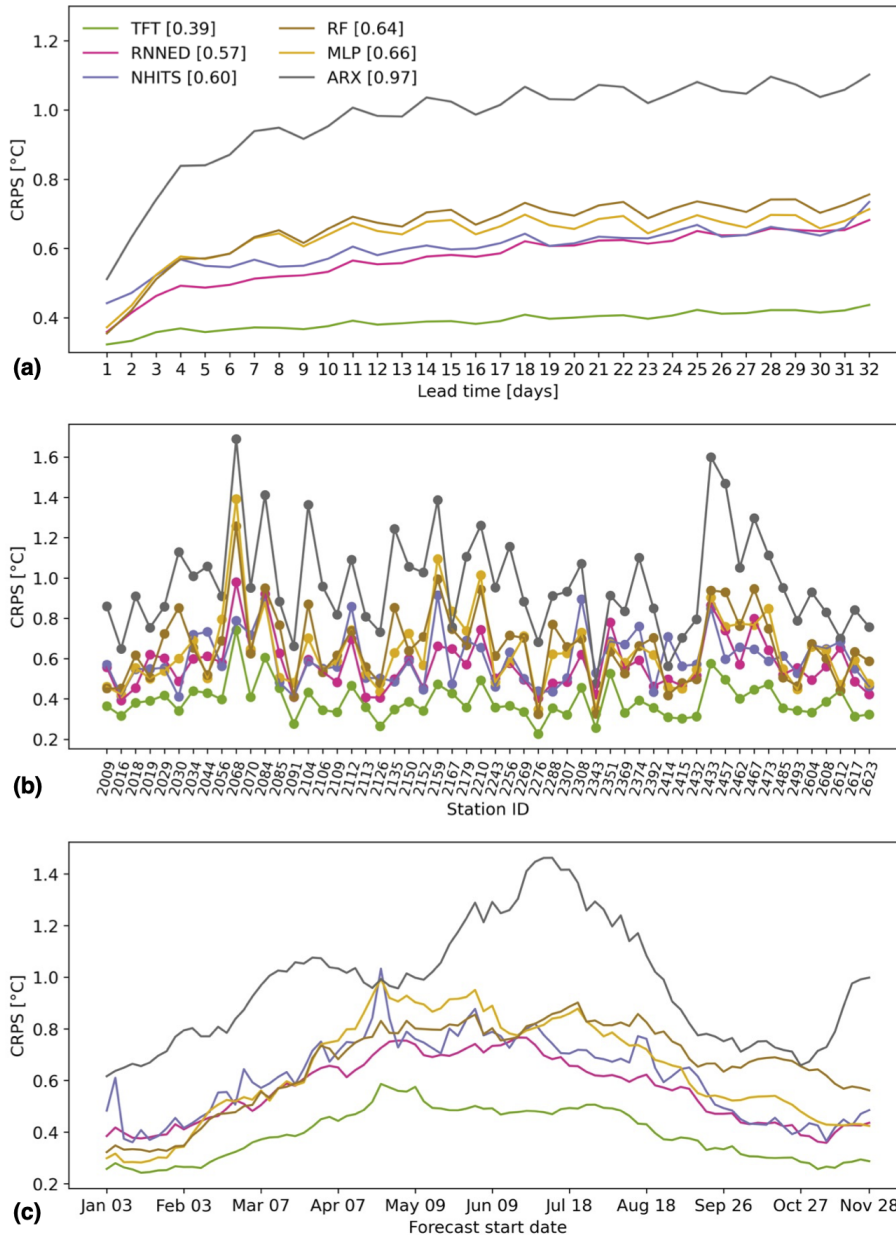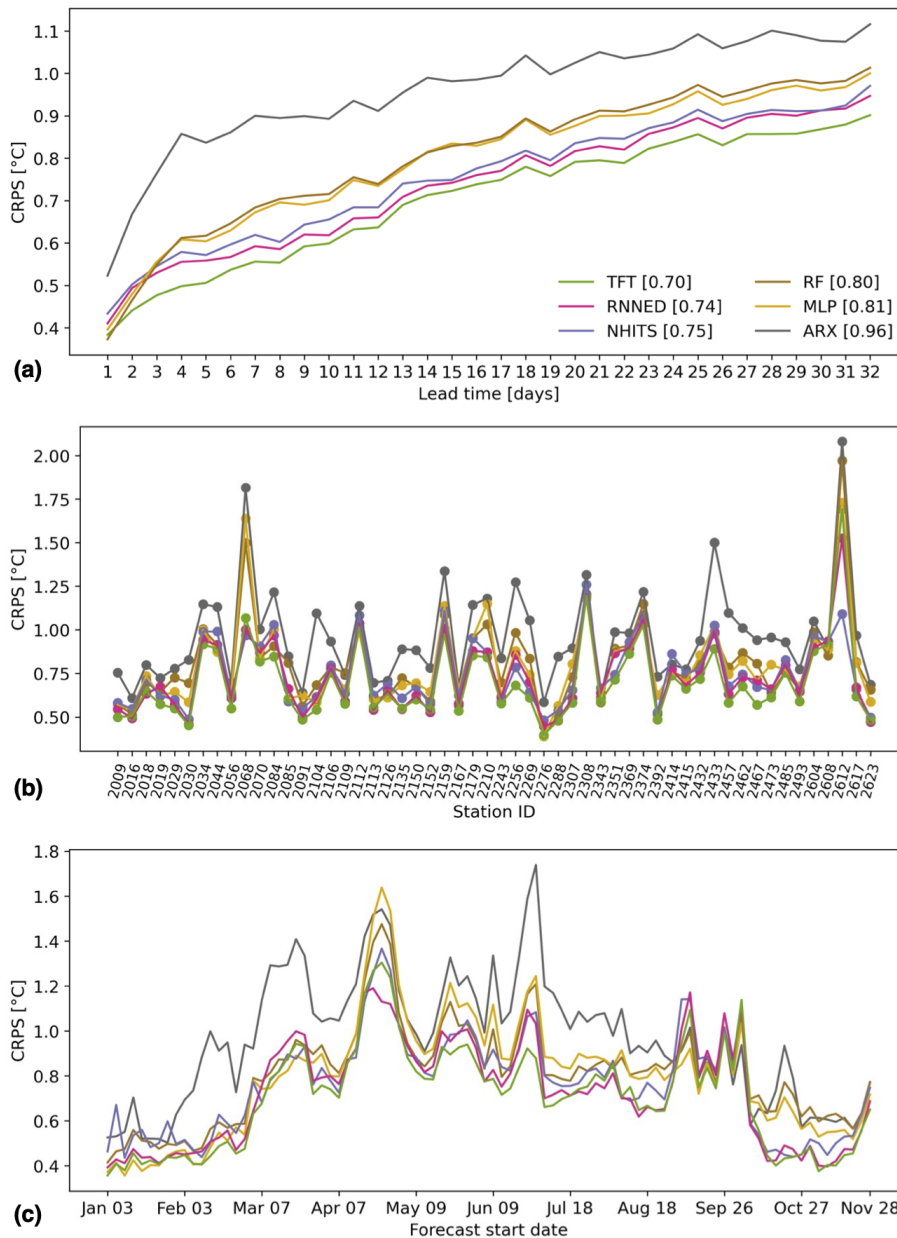
Figure 3. Model comparison of predictive skill when omitting the uncertainty of meteorological forecasts. The cumulative rank probability score (CRPS) of each model is shown as a function of **(a)** lead time averaged over all stations and forecasts, **(b)** station averaged over all lead times and forecasts, and **(c)** forecast start date averaged over all lead times and stations. The legend indicates the different models and their average CRPS over all 32 lead times, 54 stations, and 90 forecasts distributed over the year 2022.

There is a clear decrease in prediction skill across the 20 stations when forecasting with models that exclude information on past water temperature and that are trained with the data from these stations omitted (setup C) so as to represent ungauged stations (Fig. 6). Nonetheless, the TFT is still able to achieve an average CRPS of 1.29 °C across all 32 lead times, 20 stations, and 90 forecast start dates, which corresponds to a reduction in prediction skill of 0.57 °C compared to the model that includes past observations of water temperature and that is trained using data from all 54 stations. The average CRPS of the TFT at ungauged stations increases from 1.15 °C at a lead time of 1 d to 1.47 °C at a lead time of 32 d. Furthermore, the CRPS of the TFT is lower than that of the RNNED and NHITS across almost all 20 stations and 90 forecast start dates. On the other hand, it is evident that the NHITS model is not well-suited to generating predictions at ungauged stations as it relies strongly on past observations of the target variable to forecast future values.
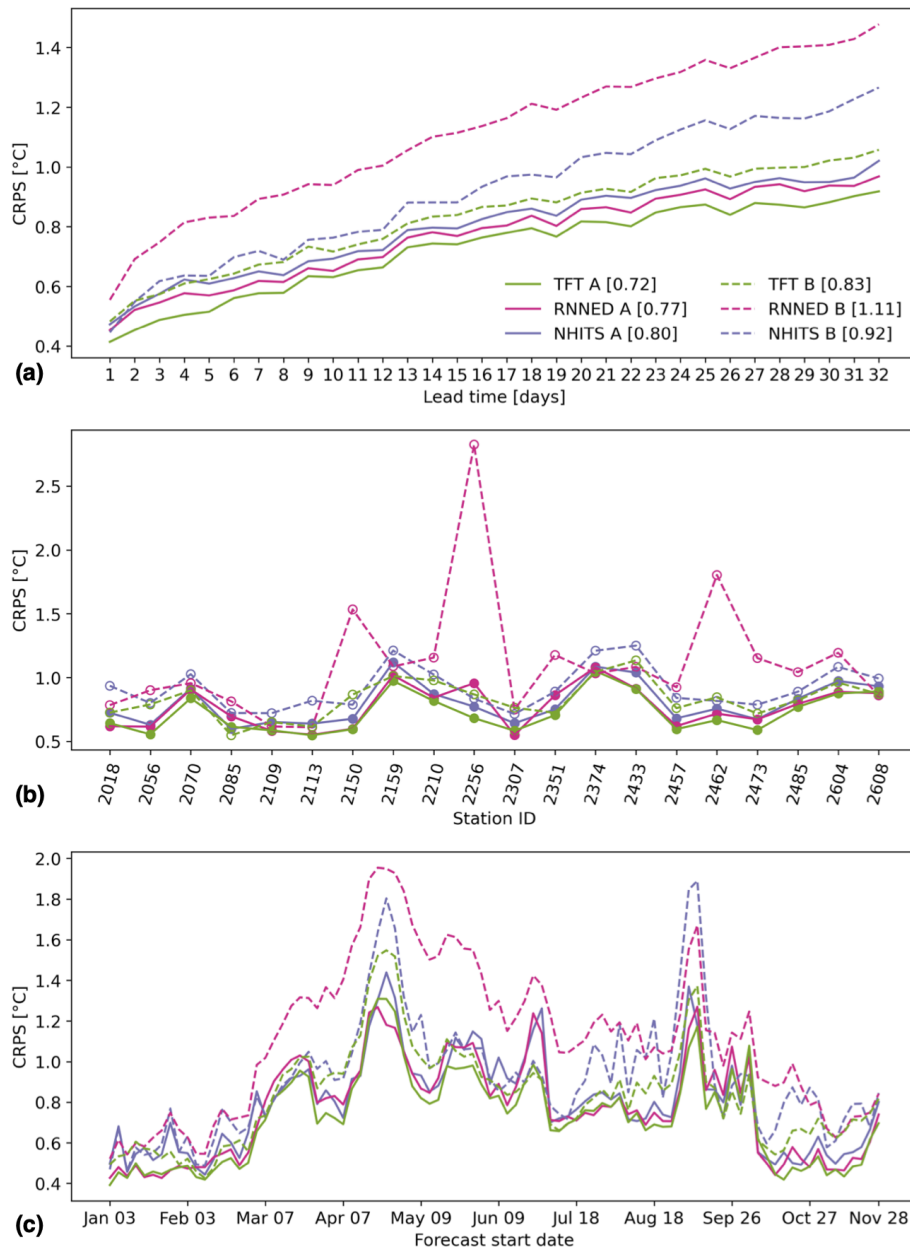
Figure 4. Model comparison of predictive skill when including the uncertainty of meteorological forecasts. The cumulative rank probability score (CRPS) of each model is shown as a function of **(a)** lead time averaged over all stations and forecasts, **(b)** station averaged over all lead times and forecasts, and **(c)** forecast start date averaged over all lead times and stations. The legend indicates the different models and their average CRPS over all 32 lead times, 54 stations, and 90 forecasts distributed over the year 2022.

3.3 Predictive importance of model inputs

Here, we focus on the TFT given the fact that it outperforms the other models and because of its built-in interpretability (Lim et al., 2021). For every forecast, the TFT directly outputs fractional importance weights (importance) that sum up to 1 for static features, for encoder features, and for decoder features separately. On average, across the 10 random seeds and 54 stations, results show similar importance values for all static features (Fig. S12). The target center (i.e., the long-term average of daily maximum water temperature) with 0.16 has the highest importance, whereas the catchment area with 0.09 has the lowest importance. For individual stations, features with higher importance are typically those that differentiate them from other stations. For example, the importance of catchment glacierized fraction increases for stations with a higher glacierized fraction.

Figure 7 shows that WT has the highest importance among the encoder features, with an average value of 0.35 over all

Figure 5. Model comparison of predictive skill at new stations. Continuous lines correspond to setup A, in which models are trained on data from all 54 stations, whereas dashed lines correspond to setup B, in which models are trained on data excluding the subset of 20 stations. The cumulative rank probability score (CRPS) of each model is shown as a function of **(a)** lead time averaged over a subset of 20 stations and all forecasts, **(b)** station averaged over all lead times and forecasts, and **(c)** forecast start date averaged over all lead times and a subset of 20 stations. The legend indicates the different models and their average CRPS over all 32 lead times, 20 stations, and 90 forecasts distributed over the year 2022.

random seeds, encoder time steps, stations, and forecasts. AT, SD, and DI have similar importance values of 0.17, 0.18, and 0.19, respectively, whereas P with 0.11 has the lowest. There is very low importance variability in the encoder features across time steps, stations, and forecast start dates. Nevertheless, we note a slightly higher importance of WT at larger catchments and a small increase in the importance

of AT for forecasts in July and August. For the decoder features, AT and DI have the highest average importance, with a value of 0.33, followed by P, with a value of 0.20, and SD, with a value of 0.14. These weights are almost constant for all decoder time steps. Across stations, we find that in approximately half of them, AT is slightly more important than DI, whereas the opposite is true for the remaining half. Also,
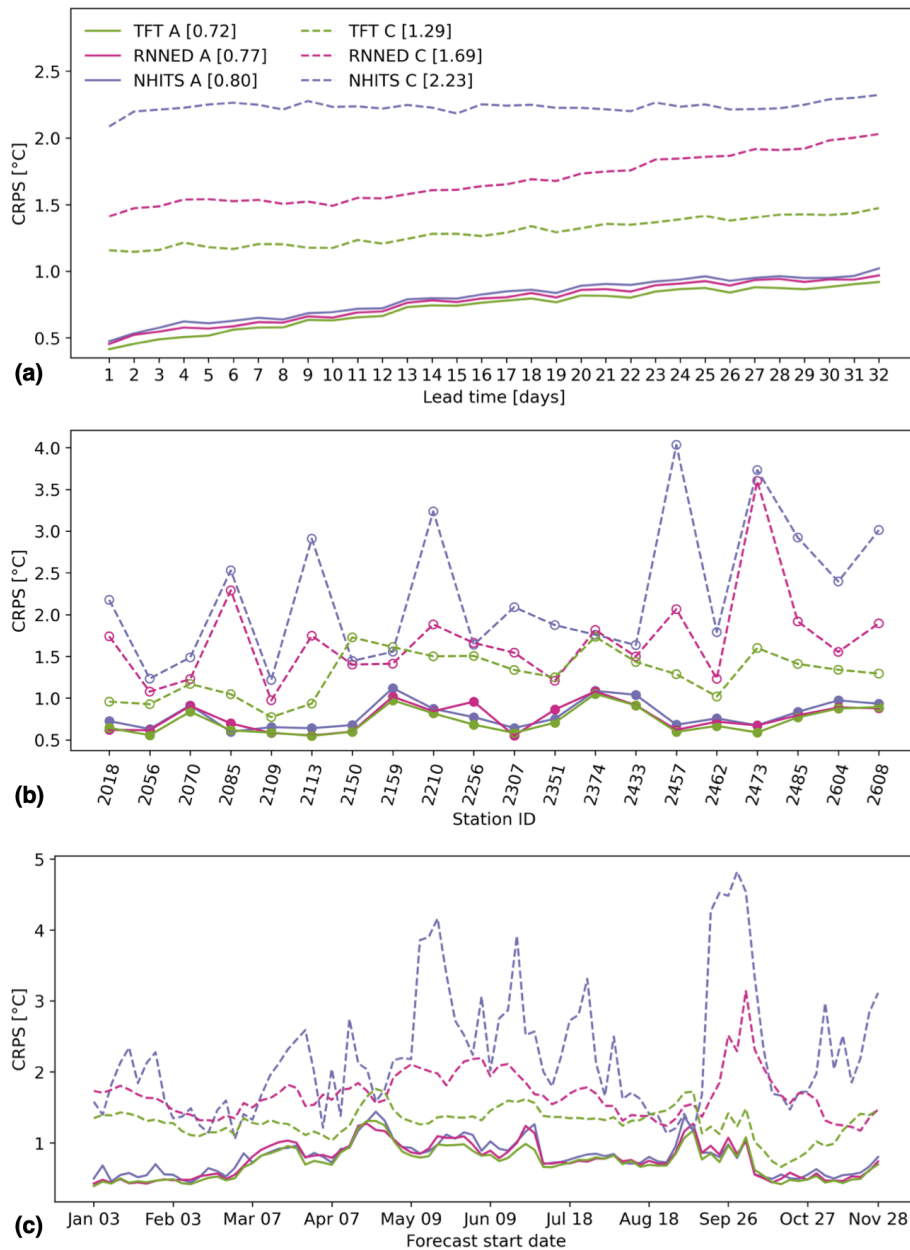
Figure 6. Model comparison of predictive skill at ungauged stations. Continuous lines correspond to setup A, in which models include past observations of water temperature as a feature and are trained on data from all 54 stations, whereas dashed lines correspond to setup C, in which models exclude past observations of water temperature as a feature and are trained on data excluding the subset of 20 stations. The cumulative rank probability score (CRPS) of each model is shown as a function of **(a)** lead time averaged over a subset of 20 stations and all forecasts, **(b)** station averaged over all lead times and forecasts, and **(c)** forecast start date averaged over all lead times and a subset of 20 stations. The legend indicates the different models and their average CRPS over all 32 lead times, 20 stations, and 90 forecasts distributed over the year 2022.

there is a small but noteworthy increase in P importance at high elevation-stations at the expense of AT. Lastly, results suggest that DI is generally more important for forecasts during the cold months, whereas the importance of AT, P, and SD increases during the warm months. The detailed insights from Fig. 7 are consistent with the global feature importance

estimates from the RF model (Fig. S13), deduced from the decrease in accuracy when randomly permuting the values of a feature.

When interpreting the importance weights, it is useful to acknowledge that the model features are clearly not independent of one another. The meteorological features correlate
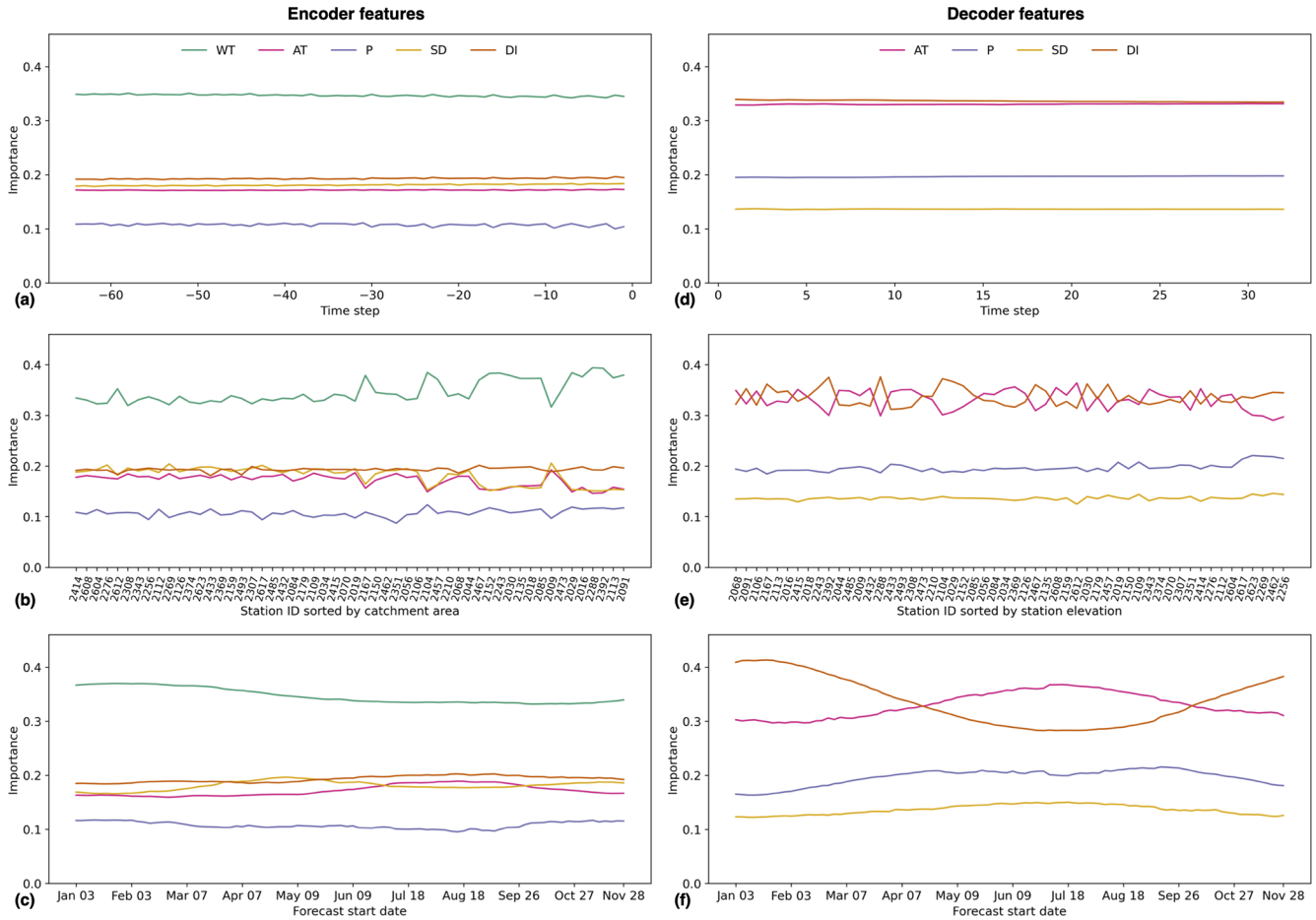
Figure 7. TFT feature importance. The importance of each feature is shown as a function of **(a, d)** time step averaged over all stations and forecasts, **(b, e)** station averaged over all time steps and forecasts, and **(c, f)** forecast start date averaged over all time steps and stations. Encoder feature importance is shown in **(a)**, **(b)**, and **(c)**, and decoder feature importance is shown in **(d)**, **(e)**, and **(f)**. Note that, in **(b)**, stations are sorted by catchment area in ascending order, and in **(e)**, stations are sorted by station elevation in ascending order. In all cases, the importance is averaged across 10 models trained with different random seeds.

with DI due to their seasonality. A higher SD is expected to coincide with a higher AT, particularly during the warmer months. In addition, cloudiness influences the number of sunny hours and is a prerequisite for precipitation, thus relating SD and P. Consequently, the feature importance values can vary substantially every time the TFT model is trained with a different random seed (Fig. S14), even though the predictive skill hardly changes. In an operational context, the importance weights are nonetheless relevant to shed light on which meteorological conditions influence the model more every time a new forecast of daily maximum water temperature is generated.

The TFT also provides fractional attention weights (attention) that sum up to 1 and indicate the relevance of information from different encoder time steps for the forecasts. On average, attention is highest for the most recent 5 d leading up to the forecast date and then rather similar from time step −6 to time step −64 (Fig. 8a). These higher attention val-

ues for the most recent days prior to the start of the forecast mainly occur for forecasts initialized in the spring and autumn (Fig. 8b). Furthermore, it is evident how the high attention of recent time steps for forecasts starting in March and April propagates to time steps further back in time over the next forecast start dates. This suggests that the values of the encoder features (WT, AT, P, SD, and DI) in spring remain relevant for forecast start dates up to 64 d later at the end of June. Given that attention weights are influenced by the importance of the model's encoder features, there is also significant attention variability for models trained with different random seeds (Fig. S15). Typically, the relative attention of time steps further back in time increases when WT and DI have higher importance, whereas the attention of most recent time steps tends to increase when the model relies more on AT and SD.

In addition to the TFT importance weights, here, we compare the predictive skill of TFT models with different sets
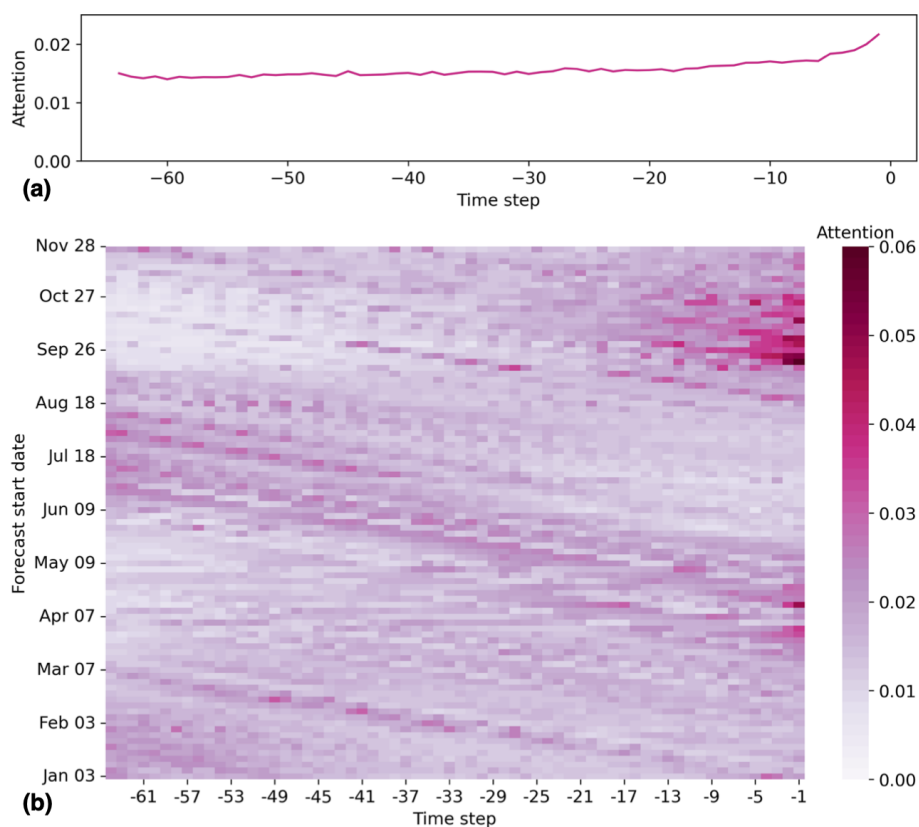
Figure 8. TFT attention weights of encoder time steps. **(a)** Attention averaged across random seeds, stations, and forecast start dates as a function of encoder time step. **(b)** Attention averaged across random seeds and stations as a function of encoder time step and forecast start date.

of predictor features (Fig. 9). When omitting the uncertainty of meteorological forecasts, results show an average CRPS of 0.51 °C for the simplest model with the following predictors: long-term average and standard deviation of WT (target center and scale) from each station as static features, encoder period WT, and AT. With each new predictor included in the model, the CRPS improves incrementally across almost all lead times, stations, and forecasts, reaching an average of 0.39 °C for the most complex model with catchment static features, P, SD, and DI as additional predictors. The largest gain in predictive skill is obtained when adding P as a predictor, with the improvement taking place mostly at stations of small and low-elevation catchments, in addition to being particularly high in spring. Given that smaller catchments tend to have less streamflow, precipitation events could more easily influence upstream water mixing and, consequently, station water temperature. Also, in spring, we expect larger water temperature differences between contributing sources such as rainfall runoff, snowmelt, and lake discharge. In addition to P, the inclusion of DI also clearly improves predictive skill by capturing seasonal characteristics of water and heat fluxes in the catchments. Overall, our findings are consistent with previous studies noting the relevance of precipitation or

runoff, as well as global radiation and time of the year, for predicting stream water temperature (Feigl et al., 2021; Zhu and Piotrowski, 2020).

The biases and spread of the ensemble meteorological forecasts limit the gain in predictive skill as more predictors are included in the TFT models. The average CRPS improves from 0.77 °C for the simplest model to 0.70 °C for the model with static features, WT (encoder period), AT, P, SD, and DI. Nevertheless, adding SD forecasts is particularly beneficial with regard to improving model skill for lead times longer than 3 weeks and at high-elevation stations such as 2256 (Rosegbach – Pontresina), 2269 (Lonza – Blatten), 2612 (Riale di Pincascia – Lavertezzo), and 2617 (Rom – Müstair). Lastly, we note that including SD and DI is especially beneficial for forecast start dates from mid-April to the end of June.

3.4 Operational forecasts

Extended-range probabilistic forecasts of daily maximum water temperature at the 54 stations in Switzerland are generated operationally twice per week and are made available at https://www.drought.ch/de/impakt-vorhersagen-malefix/wassertemperatur-prognosen/. The best-performing TFT
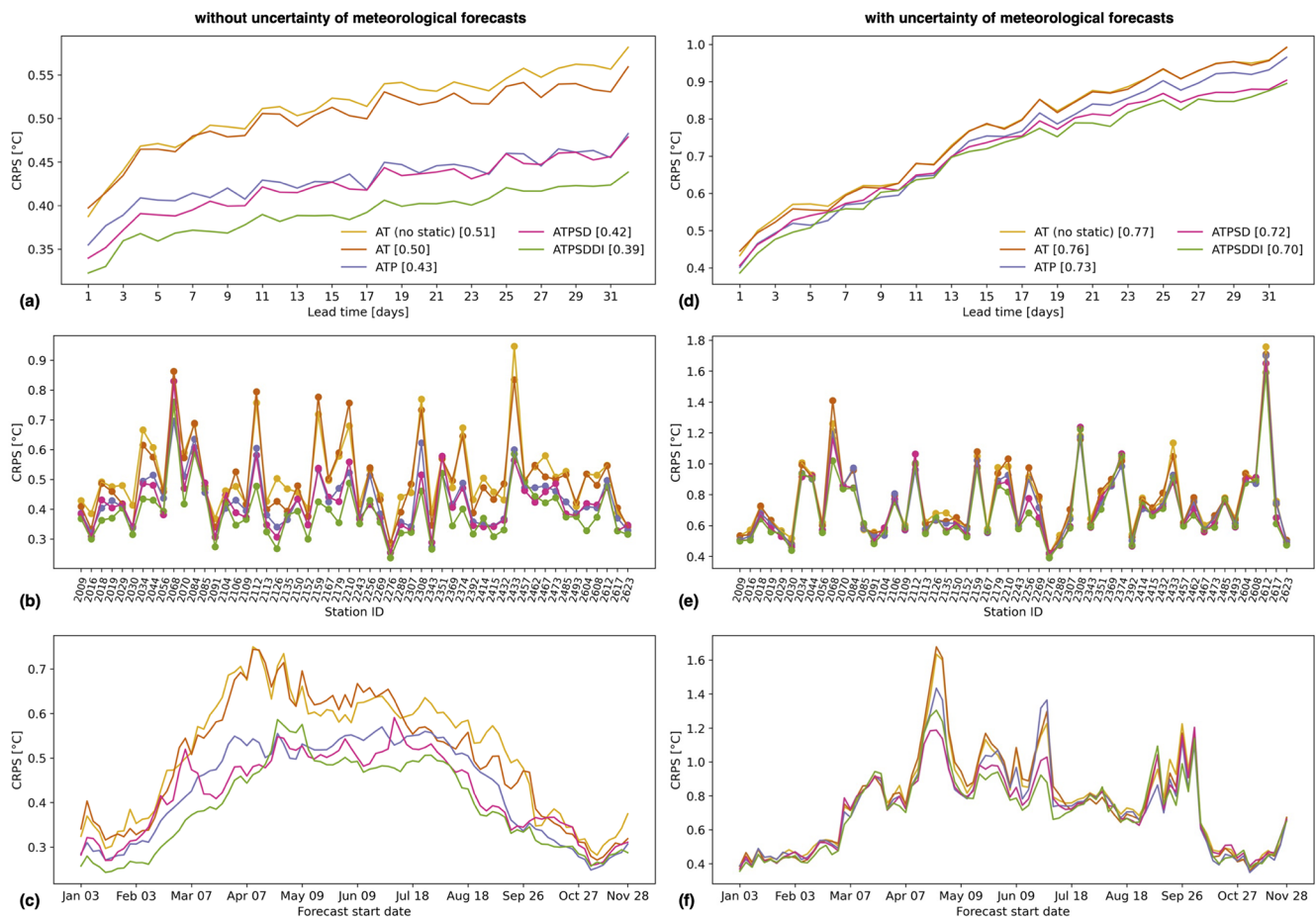
Figure 9. Predictive skill comparison of TFT models with different features. The cumulative rank probability score (CRPS) of each model is shown as a function of **(a, d)** lead time averaged over all stations and forecasts, **(b, e)** station averaged over all lead times and forecasts, and **(c, f)** forecast start date averaged over all lead times and stations. The CRPS is shown when computed with the omission of the uncertainty of meteorological forecasts **(a, b, c)** and when computed with the inclusion of the uncertainty of meteorological forecasts **(d, e, f)**. The legend indicates the different models and their average CRPS over all 32 lead times, 54 stations, and 90 forecasts distributed over the year 2022. "AT (no static)" includes the long-term average and standard deviation of WT (target center and scale) from each station as static features, encoder period WT, and AT. "AT" has the same features, as well as catchment static features (i.e., station coordinates, area, mean elevation, and glacierized fraction). "ATP" adds P as a predictor, "ATPSD" adds SD, and "ATPSDDI" adds DI.
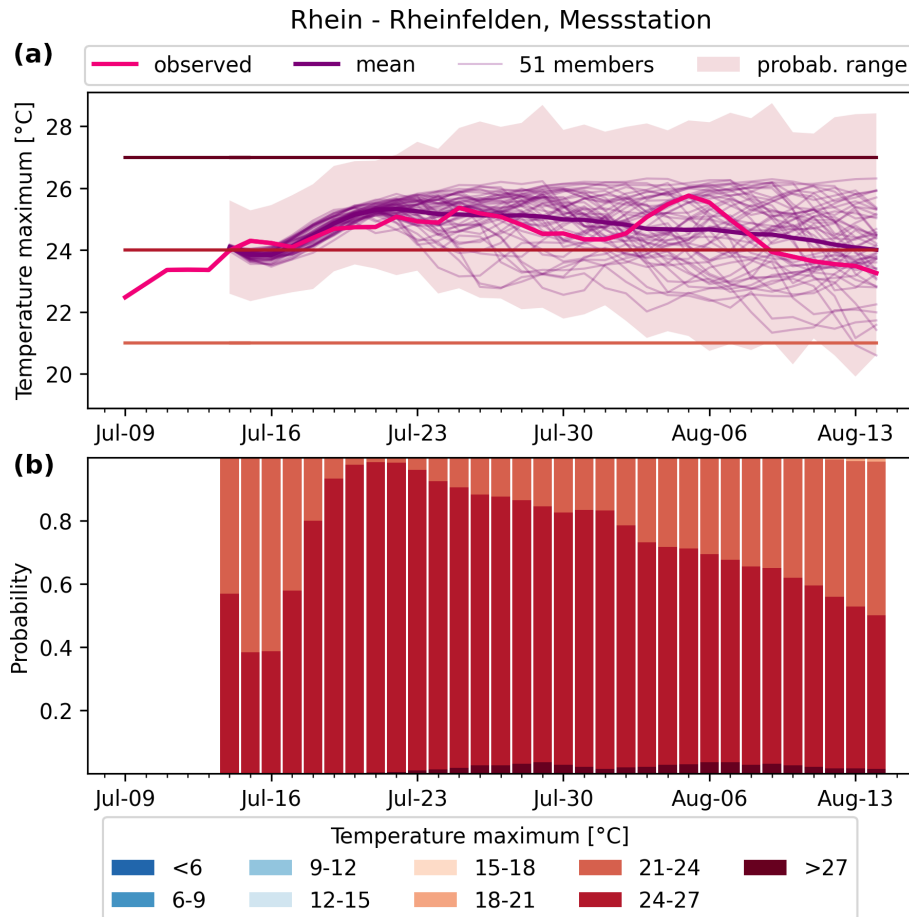
model with static catchment features, AT, P, SD, DI, and past WT as predictors is used. Figure 10 shows an example forecast for station 2091 (Rhein – Rheinfelden, Messstation) generated on 14 July 2022. Estimates based on each of the 51 ECMWF members provide insight into the expected uncertainty driven by the meteorological forecasts. The ensuing observations follow the best-estimate forecast closely during the first 7 d of lead time and remain within range up to the maximum lead time of 32 d.

It is our aim that stakeholders benefit from our timely forecasts with regard to their decision-making. As a concrete example, an early-warning system for fish thermal stress was developed using the stream water temperature forecasts as input (https://www.drought.ch/de/impakt-vorhersagen-malefix/ risiko-von-thermischem-stress-fuer-fische/, last access:

20 March 2025). High stream water temperatures pose a grave threat to fish populations (Barbarossa et al., 2021), as experienced during the summer of 2018 in Switzerland when tons of fish died in the Rhein. Therefore, timely knowledge on the exceedance potential of dangerous water temperature thresholds as given in Fig. 10 is important. The 14 July forecast indicated occurrence probabilities generally greater than 60 % for daily maximum stream water temperature to rise above 24 °C at station 2091 over the coming weeks, which was then the case from 14 July to 8 August.

4   Conclusions

In this study, we evaluate state-of-the-art deep-learning models for stream water temperature predictions over 32 d given

Figure 10. Operational daily maximum water temperature forecast on 14 July 2022 at station 2091 (Rhein – Rheinfelden, Messstation). The forecast is generated with the best-performing TFT model with static catchment features, AT, P, SD, DI, and past WT as predictors. The temporal evolution of observed water temperature is shown in **(a)** together with the forecast best estimate, the 51 estimates based on each of the ECMWF ensemble members of the meteorological forecast, and the probability range. Panel **(b)** shows the daily forecast probability for different categories of daily maximum water temperature.

the high value of skillful probabilistic extended-range forecasts for managerial decisions. Deep-learning models go beyond the iterative predictions of their standard counterparts by efficiently generating direct multi-horizon forecasts across multiple stations at once. The TFT model performs best, with an average CRPS of 0.70 °C, which is degraded from 0.38 °C at a 1 d lead time to 0.90 °C at a 32 d lead time. We find that 0.31 °C of the average disagreement between observations and predictions stems from the uncertainty in the meteorological forecasts of AT, P, and SD. This is a novel insight into the current limits of extended-range water temperature predictability.

The 54 stream water temperature stations from the Swiss Federal Office for the Environment monitoring network comprise catchments varying in size, elevation, and steepness and with different degrees of human interventions. These data are exploited by the deep-learning algorithms to generalize the relationships between water temperature and its predic-

tors. Our results demonstrate the potential of the TFT model to predict water temperature at stations on which it was not trained and at ungauged locations. The error at new stations increases by 0.11 °C, reaching an average CRPS of 0.83 °C, whereas it increases to 1.29 °C when local water temperature is unavailable to the model. This is an important step forward in the quest to expand the availability of stream water temperature estimates across the world. Furthermore, the TFT model may also be used to generate predictions under future climate scenarios assuming no major changes in how water temperature responds to changes in the meteorological drivers.

Our detailed analysis of the importance of different model inputs highlights the roles of WT in the encoder period, of AT and DI in the decoder period, and of the station-specific long-term average of daily maximum water temperature among the static features. The TFT model with only WT and AT as time-varying inputs achieves an average CRPS of 0.76 °C,

which improves to 0.70 °C when including P, SD, and DI. Overall, the TFT insights into feature importance and the attention to encoder period time steps for each forecast provide valuable interpretability that was often missing in machine learning models.

The publicly available operational system for extended-range forecasts of daily maximum water temperature completes our contribution by regularly providing information to parties interested in the consequences of extreme conditions. The methodology, insights, and product of this study help address the growing challenges surrounding stream water temperatures – and, consequently, water quality – in our warming world. Finally, we underscore the necessity for more and better information on this key environmental variable.

Author contributions. RSP, MZ, and KB conceived the idea and designed the study. RSP performed the analysis and wrote the paper, with suggestions from MZ and KB. LB led the implementation of the operational forecasts and provided technical support. KB contributed to the analysis. All the authors read and reviewed the paper.

References

Akiba, T., Sano, S., Yanase, T., Ohta, T., and Koyama, M.: Optuna: A Next-generation Hyperparameter Optimization Framework, in: Proceedings of the 25th ACM SIGKDD International Conference on Knowledge Discovery & Data Mining, KDD '19, Association for Computing Machinery, New York, NY, USA, 4–8 August 2019, 2623–2631, https://doi.org/10.1145/3292500.3330701, 2019.

Alfonso, S., Gesto, M., and Sadoul, B.: Temperature increase and its effects on fish stress physiology in the context of global warming, J. Fish Biol., 98, 1496–1508, https://doi.org/10.1111/JFB.14599, 2021.

Arora, R., Tockner, K., and Venohr, M.: Changing river temperatures in northern Germany: trends and drivers of change, Hydrol. Process., 30, 3084–3096, https://doi.org/10.1002/HYP.10849, 2016.

Barbarossa, V., Bosmans, J., Wanders, N., King, H., Bierkens, M. F. P., Huijbregts, M. A. J., and Schipper, A. M.: Threats of global warming to the world's freshwater fishes, Nat. Commun., 12, 1701, https://doi.org/10.1038/s41467-021-21655-w, 2021.

Bauer, P., Thorpe, A., and Brunet, G.: The quiet revolution of numerical weather prediction, Nature, 525, 47–55, https://doi.org/10.1038/nature14956, 2015.

Beitner, J.: PyTorch Forecasting Documentation, https://pytorch-forecasting.readthedocs.io/en/stable/# (last access: 20 March 2025), 2020.

Benyahya, L., Caissie, D., St-Hilaire, A., Ouarda, T. B. M. J., and Bobée, B.: A Review of Statistical Water Temperature Models, Can. Water Resour. J., 32, 179–192, https://doi.org/10.4296/CWRJ3203179, 2007.

Bergstra, J., Bardenet, R., Bengio, Y., and Kégl, B.: Algorithms for hyper-parameter optimization, in: Advances in Neural Information Processing Systems, vol. 24, edited by: Shawe-Taylor, J., Zemel, R., Bartlett, P., Pereira, F., and Weinberger, K. Q., Curran Associates, Inc., ISBN 9781618395993, 2011.

Bogner, K., Chang, A. Y. Y., Bernhard, L., Zappa, M., Monhart, S., and Spirig, C.: Tercile Forecasts for Extending the Horizon of Skillful Hydrological Predictions, J. Hydrometeorol., 23, 521–539, https://doi.org/10.1175/JHM-D-21-0020.1, 2022.

Booker, D. J., Whitehead, A. L., Doug Booker, C. J., and Modelling, F.: River water temperatures are higher during lower flows after accounting for meteorological variability, River Res. Appl., 38, 3–22, https://doi.org/10.1002/RRA.3870, 2022.

Cannon, A.: qrnn: Quantile Regression Neural Network, R package, version 2.1.1, CRAN [code], https://doi.org/10.32614/CRAN.package.qrnn, 2024.

Caretta, M. A., Mukherji, A., Arfanuzzaman, M., Betts, R. A., Gelfan, A., Hirabayashi, Y., Lissner, T. K., Liu, J., Lopez Gunn, E., Morgan, R., Mwanga, S., and Supratid, S.: Water, in: Climate Change 2022: Impacts, Adaptation and Vulnerability. Contribution of Working Group II to the Sixth Assessment Report of the Intergovernmental Panel on Climate Change, edited by: Pörtner, H.-O., Roberts, D. C., Tignor, M., Poloczanska, E. S., Mintenbeck, K., Alegría, A., Craig, M., Langsdorf, S., Löschke,

S., Möller, V., Okem, A., and Rama, B., Cambridge University Press, Cambridge, UK and New York, NY, USA, 551–712, https://doi.org/10.1017/9781009325844.006, 2022.

Challu, C., Olivares, K. G., Oreshkin, B. N., Ramirez, F. G., Mergenthaler-Canseco, M., and Dubrawski, A.: NHITS: Neural Hierarchical Interpolation for Time Series Forecasting, in: Proceedings of the AAAI Conference on Artificial Intelligence, Washington DC, USA, 7–14 February 2023, 37, 6989–6997, https://doi.org/10.1609/AAAI.V37I6.25854, 2023.

Chang, A. Y. Y., Bogner, K., Grams, C. M., Monhart, S., Domeisen, D. I. V., and Zappa, M.: Exploring the Use of European Weather Regimes for Improving User-Relevant Hydrological Forecasts at the Subseasonal Scale in Switzerland, J. Hydrometeorol., 24, 1597–1617, https://doi.org/10.1175/JHM-D-21-0245.1, 2023.

Chapra, S. C., Camacho, L. A., and McBride, G. B.: Impact of Global Warming on Dissolved Oxygen and BOD Assimilative Capacity of the World's Rivers: Modeling Analysis, Water, 13, 2408, https://doi.org/10.3390/W13172408, 2021.

Cho, K., Van Merriënboer, B., Gulcehre, C., Bahdanau, D., Bougares, F., Schwenk, H., and Bengio, Y.: Learning Phrase Representations using RNN Encoder-Decoder for Statistical Machine Translation, EMNLP 2014 – 2014 Conference on Empirical Methods in Natural Language Processing, Proceedings of the Conference, Doha, Qatar, 25–29 October 2014, 1724–1734, https://doi.org/10.3115/v1/d14-1179, 2014.

Clevert, D. A., Unterthiner, T., and Hochreiter, S.: Fast and Accurate Deep Network Learning by Exponential Linear Units (ELUs), 4th International Conference on Learning Representations, ICLR 2016 – Conference Track Proceedings, San Juan, Puerto Rico, 2–4 May 2016, https://doi.org/10.48550/arXiv.1511.07289, 2016.

Comer-Warner, S. A., Gooddy, D. C., Ullah, S., Glover, L., Percival, A., Kettridge, N., and Krause, S.: Seasonal variability of sediment controls of carbon cycling in an agricultural stream, Sci. Total Environ., 688, 732–741, https://doi.org/10.1016/J.SCITOTENV.2019.06.317, 2019.

Corona, C. R. and Hogue, T. S.: Machine Learning in Stream/River Water Temperature Modelling: a review and metrics for evaluation, Hydrol. Earth Syst. Sci. Discuss. [preprint], https://doi.org/10.5194/hess-2024-256, in review, 2024.

Dugdale, S. J., Hannah, D. M., and Malcolm, I. A.: River temperature modelling: A review of process-based approaches and future directions, Earth Sci. Rev., 175, 97–113, https://doi.org/10.1016/J.EARSCIREV.2017.10.009, 2017.

Elliott, J. M. and Elliott, J. A.: Temperature requirements of Atlantic salmon Salmo salar, brown trout Salmo trutta and Arctic charr Salvelinus alpinus: predicting the effects of climate change, J. Fish Biol., 77, 1793–1817, https://doi.org/10.1111/J.1095-8649.2010.02762.X, 2010.

Fakoor, R., Kim, T., Mueller, J., Cleanlab, J. A., Smola, A. J., and Tibshirani, R. J.: Flexible model aggregation for quantile regression, J. Mach. Learn. Res., 24, 1–45, http://jmlr.org/papers/v24/22-0799.html (last access: 20 March 2025), 2023.

Fan, C., Zhang, Y., Pan, Y., Li, X., Zhang, C., Yuan, R., Wu, D., Wang, W., Pei, J., and Huang, H.: Multi-horizon time series forecasting with temporal attention learning, in: Proceedings of the ACM SIGKDD International Conference on Knowledge Discovery and Data Mining, Anchorage AK, USA, 4–8 August 2019, 2527–2535, https://doi.org/10.1145/3292500.3330662, 2019.

Feigl, M., Lebiedzinski, K., Herrnegger, M., and Schulz, K.: Machine-learning methods for stream water temperature prediction, Hydrol. Earth Syst. Sci., 25, 2951–2977, https://doi.org/10.5194/hess-25-2951-2021, 2021.

Ficklin, D. L., Hannah, D. M., Wanders, N., Dugdale, S. J., England, J., Klaus, J., Kelleher, C., Khamis, K., and Charlton, M. B.: Rethinking river water temperature in a changing, human-dominated world, Nature Water, 1, 125–128, https://doi.org/10.1038/s44221-023-00027-2, 2023.

Hannah, D. M. and Garner, G.: River water temperature in the United Kingdom: Changes over the 20th century and possible changes over the 21st century, Prog. Phys. Geogr., 39, 68–92, https://doi.org/10.1177/0309133314550669, 2015.

Hannah, D. M., Webb, B. W., and Nobilis, F.: River and stream temperature: dynamics, processes, models and implications – preface, Hydrol. Process., 22, 899–901, 2008.

Hannah, D. M., Demuth, S., van Lanen, H. A. J., Looser, U., Prudhomme, C., Rees, G., Stahl, K., and Tallaksen, L. M.: Large-scale river flow archives: importance, current status and future needs, Hydrol. Process., 25, 1191–1200, https://doi.org/10.1002/HYP.7794, 2011.

Hardenbicker, P., Viergutz, C., Becker, A., Kirchesch, V., Nilson, E., and Fischer, H.: Water temperature increases in the river Rhine in response to climate change, Reg. Environ. Change, 17, 299–308, https://doi.org/10.1007/s10113-016-1006-3, 2017.

Hochreiter, S. and Schmidhuber, J.: Long Short-Term Memory, Neural Comput, 9, 1735–1780, https://doi.org/10.1162/NECO.1997.9.8.1735, 1997.

Johnson, M. F., Albertson, L. K., Algar, A. C., Dugdale, S. J., Edwards, P., England, J., Gibbins, C., Kazama, S., Komori, D., MacColl, A. D. C., Scholl, E. A., Wilby, R. L., de Oliveira Roque, F., and Wood, P. J.: Rising water temperature in rivers: Ecological impacts and future resilience, WIREs Water, 11, e1724, https://doi.org/10.1002/WAT2.1724, 2024.

Jollife, I. T. and Stephenson, D. B.: Forecast verification. A practitioner's guide in atmospheric science, 2nd edn., Wiley-Blackwell, UK, ISBN 9780470660713, eISBN 9781119960003, 2012.

Kelleher, C. A., Golden, H. E., and Archfield, S. A.: Monthly river temperature trends across the US confound annual changes, Environ. Res. Lett., 16, 104006, https://doi.org/10.1088/1748-9326/AC2289, 2021.

Kraft, B., Schirmer, M., Aeberhard, W. H., Zappa, M., Seneviratne, S. I., and Gudmundsson, L.: CH-RUN: a deep-learning-based spatially contiguous runoff reconstruction for Switzerland, Hydrol. Earth Syst. Sci., 29, 1061–1082, https://doi.org/10.5194/hess-29-1061-2025, 2025.

Laio, F. and Tamea, S.: Verification tools for probabilistic forecasts of continuous hydrological variables, Hydrol. Earth Syst. Sci., 11, 1267–1277, https://doi.org/10.5194/hess-11-1267-2007, 2007.

Li, L., Jamieson, K., DeSalvo, G., Rostamizadeh, A., and Talwalkar, A.: Hyperband: A Novel Bandit-Based Approach to Hyperparameter Optimization, J. Mach. Learn. Res., 18, 1–52, http://jmlr.org/papers/v18/16-558.html (last access: 20 March 2025), 2018.

Lim, B., Arık, S., Loeff, N., and Pfister, T.: Temporal Fusion Transformers for interpretable multi-horizon time

series forecasting, Int. J. Forecast., 37, 1748–1764, https://doi.org/10.1016/J.IJFORECAST.2021.03.012, 2021.

Little, A. G., Loughland, I., and Seebacher, F.: What do warming waters mean for fish physiology and fisheries?, J. Fish Biol., 97, 328–340, https://doi.org/10.1111/JFB.14402, 2020.

Meinshausen, N.: Quantile Regression Forests, J. Mach. Learn. Res., 7, 983–999, 2006.

Michel, A., Brauchli, T., Lehning, M., Schaefli, B., and Huwald, H.: Stream temperature and discharge evolution in Switzerland over the last 50 years: annual and seasonal behaviour, Hydrol. Earth Syst. Sci., 24, 115–142, https://doi.org/10.5194/hess-24-115-2020, 2020.

Michel, A., Schaefli, B., Wever, N., Zekollari, H., Lehning, M., and Huwald, H.: Future water temperature of rivers in Switzerland under climate change investigated with physics-based models, Hydrol. Earth Syst. Sci., 26, 1063–1087, https://doi.org/10.5194/hess-26-1063-2022, 2022.

Ouarda, T. B. M. J., Charron, C., and St-Hilaire, A.: Regional estimation of river water temperature at ungauged locations, J. Hydrol. X, 17, 100133, https://doi.org/10.1016/J.HYDROA.2022.100133, 2022.

Ouellet, V., St-Hilaire, A., Dugdale, S. J., Hannah, D. M., Krause, S., and Proulx-Ouellet, S.: River temperature research and practice: Recent challenges and emerging opportunities for managing thermal habitat conditions in stream ecosystems, Sci. Total Environ., 736, 139679, https://doi.org/10.1016/J.SCITOTENV.2020.139679, 2020.

Ouellet-Proulx, S., St-Hilaire, A., and Boucher, M. A.: Water Temperature Ensemble Forecasts: Implementation Using the CEQUEAU Model on Two Contrasted River Systems, Water, 9, 457, https://doi.org/10.3390/W9070457, 2017.

Padrón Flasher, R., Zappa, M., Bernhard, L., and Bogner, K.: Scripts for the article "Extended range forecasting of stream water temperature with deep learning models", ETH Zürich Research Collection [code], https://doi.org/10.3929/ethz-b-000718530, 2025.

Qiu, R., Wang, Y., Rhoads, B., Wang, D., Qiu, W., Tao, Y., and Wu, J.: River water temperature forecasting using a deep learning method, J. Hydrol., 595, 126016, https://doi.org/10.1016/J.JHYDROL.2021.126016, 2021.

Singh, G. G., Sajid, Z., and Mather, C.: Quantitative analysis of mass mortality events in salmon aquaculture shows increasing scale of fish loss events around the world, Scientific Reports, 14, 3763, https://doi.org/10.1038/s41598-024-54033-9, 2024.

Toffolon, M. and Piccolroaz, S.: A hybrid model for river water temperature as a function of air temperature and discharge, Environ. Res. Lett., 10, 114011, https://doi.org/10.1088/1748-9326/10/11/114011, 2015.

Tripathy, K. P. and Mishra, A. K.: Deep learning in hydrology and water resources disciplines: concepts, methods, applications, and research directions, J. Hydrol., 130458, https://doi.org/10.1016/J.JHYDROL.2023.130458, 2023.

van Vliet, M. T. H., Franssen, W. H. P., Yearsley, J. R., Ludwig, F., Haddeland, I., Lettenmaier, D. P., and Kabat, P.: Global river discharge and water temperature under climate change, Global Environ. Change, 23, 450–464, https://doi.org/10.1016/J.GLOENVCHA.2012.11.002, 2013.

van Vliet, M. T. H., Florke, M., and Wada, Y.: Quality matters for water scarcity, Nat. Geosci., 10, 800–802, https://doi.org/10.1038/ngeo3047, 2017.

van Vliet, M. T. H., Thorslund, J., Strokal, M., Hofstra, N., Flörke, M., Ehalt Macedo, H., Nkwasa, A., Tang, T., Kaushal, S. S., Kumar, R., van Griensven, A., Bouwman, L., and Mosley, L. M.: Global river water quality under climate change and hydroclimatic extremes, Nature Reviews Earth & Environment, 4, 687–702, https://doi.org/10.1038/s43017-023-00472-3, 2023.

Wade, J., Kelleher, C., and Hannah, D. M.: Machine learning unravels controls on river water temperature regime dynamics, J. Hydrol., 623, 129821, https://doi.org/10.1016/J.JHYDROL.2023.129821, 2023.

Webb, B. W.: Trends in stream and river temperature, Hydrol. Process., 10, 205–226, https://doi.org/10.1002/(SICI)1099-1085(199602)10:2<205::AID-HYP358>3.0.CO;2-1, 1996.

Wen, R., Torkkola, K., Narayanaswamy, B., and Madeka, D.: A Multi-Horizon Quantile Recurrent Forecaster, in: 31st Conference on Neural Information Processing Systems (NIPS 2017), Time Series Workshop, Long Beach, CA, USA, 4–9 December 2017, https://doi.org/10.48550/arXiv.1711.11053, 2018.

Wright, M. N. and Ziegler, A.: Ranger: A fast implementation of random forests for high dimensional data in C++ and R, J. Stat. Softw., 77, 1–17, https://doi.org/10.18637/JSS.V077.I01, 2017.

Zhu, S. and Piotrowski, A. P.: River/stream water temperature forecasting using artificial intelligence models: a systematic review, Acta Geophys., 68, 1433–1442, https://doi.org/10.1007/S11600-020-00480-7, 2020.